Active Terahertz Spoof Surface Plasmon Polariton Switch Comprising the Perfect Conductor Metamaterial

Kyungjun Song and Pinaki Mazumder, *Fellow, IEEE*

Abstract—The feasibility of realizing an active terahertz (THz) switch by utilizing artificially corrugated perfect conductor metamaterials is reported in this paper by demonstrating that the strongly localized THz spoof surface plasmon polariton (SSPP) modes can be easily controlled by changing the refractive index of dielectrics inside a longitudinal metallic structure with a periodic array of grooves. Specifically, this paper shows that incorporation of electrooptical material such as a *nematic liquid crystal* into the plasmonic gap leads to a highly compact and efficient THz switch that is activated by a low-voltage control-signal. The optimal design of the SSPP switch enabled by this novel method shows: 1) a strong subwavelength SSPP localization; 2) relatively high extinction ratio; and 3) small damping attenuation. Furthermore, the design flexibility associated with simple micrometer-scale architecture provides a promising method toward controlling or steering the subwavelength THz signal in the future SSPP-based compact digital circuit.

Index Terms—Active circuit, bandwidth, nematic liquid crystal (N-LC), spoof surface plasmon polariton (SSPP), terahertz (THz).

I. INTRODUCTION

EVEN THOUGH the terahertz (THz) frequency (0.1–3 THz) remains an underexploited regime in the electromagnetic (EM) spectrum and very little commercial products operating in the THz domain have penetrated in the market, the THz EM spectrum has recently evoked a considerable interest among device and circuit researchers. New investigations are currently underway to identify future promising applications like astronomical remote sensing, medical imaging systems, military detection, and ultrafast computer logic circuit [1]–[3]. Specifically, as a basic building block for THz family of devices, passive elements such as waveguide, ring resonator, and filter are now being explored as components for the next generation of integrated circuits. Unfortunately, the conventional index-guiding methods such as plastic ribbons and sapphire fibers are not suitable for THz guiding or focusing, because of their high signal power loss [4]. As an alternative to solving the damping problems, simple metal wire was recently developed for guiding THz radiation in the form of surface plasmon polariton (SPP) that propagates at the interfacial surface between a dielectric and a metal [5]. Compared to dielectric-based waveguides, the THz SPP wave offers low loss and low dispersion. Therefore, metallic structures for carrying THz signal have gained considerable attention for THz passive elements.

However, a simple metal wire supports weakly guided THz waves because of negligible field penetration into the metallic side in comparison to the dielectric matrix surrounding the metallic wire. To overcome the weak SPP confinement in the THz domain, surface topology engineering can be employed to create holes, grooves, and dimples which mimic realistic SPP behavior at the visible or ultraviolet spectrum [6], [7]. The resulting spoof SPP (SSPP) modes enhance the subwavelength confinement on the metal surface by generating highly localized surface bound modes in the perfect conductor [8]–[10]. In this paper, we demonstrate how to build efficient THz passive circuit by utilizing these mimicking SSPP bound modes [11], [12]. However, to perform more complex signal routing and process arbitrary Boolean functions, the integrated circuit devices will require dynamic control of the guided THz signal [13]. Specifically, the active SPP circuit operating in the near infrared or optical frequency spectrum have been demonstrated and currently being explored by using some innovative methods such as electrooptical (EO), thermooptical, and all-optical devices [14], [15]. Furthermore, dynamic control of SPP modes in the lower frequency domain can be accomplished by using optical or thermal control on corrugated semiconductor structure [16]. This will open a promising possibility for controlling SPP signal and three-terminal SPP devices.

In this paper, we present a novel way to obtain an active THz SSPP switch or modulator in the perfect conductor. More recently in the literature, it is reported that the highly localized SSPP bound modes along the corrugated metallic wire can be controlled by varying its geometrical dimensions such as radius or height [12], [17]. In addition to the geometry-based method, the dynamic control of the SSPP modes can be achieved by changing the refractive index of the indentation of the grooves or the host matrix. Here, we demonstrate that the TM dispersion relation of surface-bound modes in the perfect conductor limit can be tailored by changing the refractive index of the grooves.

K. Song is with the University of Michigan, Ann Arbor, MI 48109 USA (e-mail: songk@umich.edu).

P. Mazumder is with the University of Michigan, Ann Arbor, MI 48109 USA, and also with the U.S. National Science Foundation, 4201 Wilson Boulevard, Arlington, VA 22230 USA (e-mail: mazum@eecs.umich.edu; pmazumde@nsf.gov).
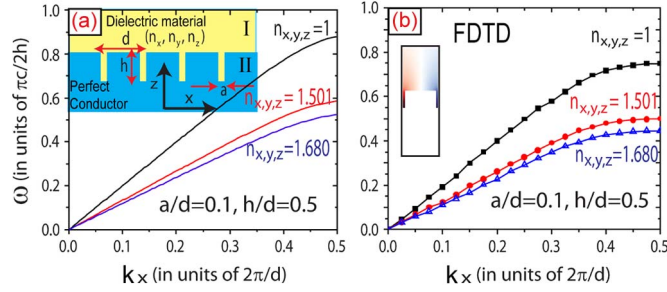
Fig. 1. (a) Dispersion diagram of SSPP modes calculated from (7). (b) Dispersion diagram of SSPP modes calculated from FDTD. The structure is supported by a 1-D array of grooves with geometrical parameters $a/d = 0.1$ and $h/d = 0.5$.

Specifically, the incorporation of *nematic* liquid crystal (N-LC) into the plasmonic gap structure, where the SSPP bound modes propagate in the dielectric gap between two textured perfect conducting surfaces, allows the device to modulate the resonant frequency of the Fabry–Pérot-like wave [18] depending on the LC orientation. This simple principle enables us to design active THz SSPP switches and modulators that are activated by electrically or optically controlled birefringence.

II. DISPERSION DIAGRAM OF SSPP ALONG THE CORRUGATED PERIODIC METAMATERIAL

The inset of Fig. 1(a) schematically shows a perfectly conducting surface that is corrugated periodically with the linearly spaced rectangular grooves that are infinite in y-direction and have height h, width a, and periodic lattice distance d. Moreover, the permittivity of Region I and grooves have anisotropic permittivity (n_x, n_y, n_z). First, we are interested in calculating the dispersion relation of TM-polarized waves propagating in the x-direction along the corrugated wave structure bounded by anisotropic dielectric material (n_x, n_y, n_z). To analyze the TM dispersion analysis as a quasi-analytical form, the EM modes can be expanded in terms of Floquet modes that are characteristic waves for periodic structures. The H field with TM polarization (magnetic field perpendicular to the plane of grating structure in Region I) may be expressed in terms of modes

$$H_y^I = \sum_{n=-\infty}^{\infty} \rho_n \exp\left(jk_{z,I}^{(n)}z\right) \exp\left(jk_{x,I}^{(n)}x\right) \qquad (1)$$

where ρ_n are amplitude of diffractions $k_{x,I}^{(n)} = k_x + 2\pi n/d$ and $(k_{x,I}^{(n)}/n_z)^2 + (k_{z,I}^{(n)}/n_x)^2 = (\omega/c)^2$ account for biaxial index ellipsoids with $n_x^2 = \epsilon_x/\epsilon_0$, $n_y^2 = \epsilon_y/\epsilon_0$, $n_z^2 = \epsilon_z/\epsilon_0$ and c is the velocity of light. On the other hand, the circular normal surface $(k_{x,I}^{(n)2} + k_{z,I}^{(n)2})/n_y^2 = (\omega/c)^2$ represents the TE polarization wave. The detail derivation of the normal surfaces in anisotropic media is described in the Appendix. Notably, in Region II, all fields are zero except inside the grooves $(-a/2 \le x \le a/2)$ of the perfect conductor, thus H_y within the grooves

can be written as a linear combination of the backward and forward z-directional TM modes

$$H_y^{II} = A^+ \exp(jk_{z,II}z) + A^- \exp(-jk_{z,II}z) \qquad (2)$$

where A^+ and A^- are constants and $k_{z,II} = n_x\omega/c$ (in the case of TE polarization: $k_{z,II} = n_y\omega/c$). It is straightforward to show that the dispersion relation of TM polarized surface wave propagating in x-direction along the periodically corrugated metamaterial can be rigorously derived by applying the boundary conditions: tangential E and H fields at the interface between Region I and II, tangential E fields vanishing at the perfect conductor surface and E-fields at the bottom of the grooves $(z = h)$. From the boundary condition, the following equations can be obtained by:

$$\sum_{n=-\infty}^{\infty} \frac{k_{z,II}S_n^2}{k_z^{(n)}}(A^+ - A^-) = (A^+ + A^-)$$

$$A^+ \exp(jk_{II,z}h) = A^- \exp(-jk_{II,z}h) \qquad (3)$$

where $S_n = (1/\sqrt{ad})\int_{-a/2}^{a/2} \exp(jk_x^{(n)}x)dx$ which is solved to show that $S_n = \sqrt{a/d}\sin c(k_x^{(n)}a/2)$. We can obtain constitutive matrix with the form of a matrix equation: $Q \times A = 0$, i.e.,

$$\begin{bmatrix} \sum \frac{S_n^2 k_{z,II}}{k_{z,I}^{(n)}} - 1 & -\sum \frac{S_n^2 k_{z,II}}{k_{z,I}^{(n)}} - 1 \\ \exp(jk_{z,II}h) & -\exp(jk_{z,II}h) \end{bmatrix} \begin{bmatrix} A^+ \\ A^- \end{bmatrix} = \begin{bmatrix} 0 \\ 0 \end{bmatrix}. \qquad (4)$$

The TM dispersion relation can be obtained in the condition of $\det Q = 0$, i.e.,

$$1 - j\sum_n \left(\frac{k_{z,II}S_n^2}{k_{z,I}^{(n)}}\right)\tan(k_{z,II}h) = 0 \qquad (5)$$

where j is $\sqrt{-1}$ and $S_n = \sqrt{a/d}\sin c(k_x^{(n)}a/2)$. With the help of the surface bound condition $(k_x > n_z\omega/c)$ and the subwavelength limit $(\lambda \gg d$ and $h)$, the zero order $(n = 0)$ dominates among all other diffraction modes. Thus, the TM dispersion relation of surface bound modes can be simplified as

$$\sqrt{n_x^2\frac{k_x^2}{n_z^2} - n_x^2\frac{\omega^2}{c^2}} = n_x\frac{\omega}{c}S_0^2\tan\left(\frac{n_x\omega h}{c}\right). \qquad (6)$$

In the limit $k_x a \ll 1$, (6) becomes

$$k_x \approx n_z\frac{\omega}{c}\sqrt{1 + \left(\frac{a}{d}\right)^2\tan^2\left(\frac{n_x\omega h}{c}\right)}. \qquad (7)$$

As a simple form, in the case of $n_x = n_y = n_z = 1$, (7) coincides with that in [19, eq. (14)], explaining the behavior for $\omega(k_x)$ in the air grooves $(n = 1)$. Note that the TM dispersion relation of SSPP modes not only depends on the geometrical parameters but also relies on the refractive indices of grooves and on Region I. In detail, the cutoff SSPP frequency $\omega_c = \pi c/2n_x h$ calculated from (5) is controlled by the depth of grooves h and the x-directional refractive index n_x. Recently, the cutoff frequency ω_c on periodically corrugated metal wires also shown to be inversely proportional to the depth of radial

grooves [12]. To demonstrate the effect of the refractive index, Fig. 1 shows the TM dispersion relation for SSPP bound modes supported by a periodically corrugated perfect conductor with geometrical parameters $a/d = 0.1$ and $h/d = 0.5$. Three different isotropic refractive indices are analyzed: $n_{x,y,z} = 1$, $n_{x,y,z} = 1.501$, and $n_{x,y,z} = 1.680$. For SSPP modes, at the long wavelength ($\lambda \gg d$), the dispersion curves asymptotically approach the light line $k_x = n_z \omega/c$ because the EM wave does not recognize the fine periodic structure. However, as the frequency increases up to the cutoff frequency ω_c, the highly localized surface bound modes are generated along the textured structure. In addition, Fig. 1(b) shows the dispersion diagram of SSPP modes calculated from FDTD. These band diagrams can be analyzed in the form of periodic Bloch modes, which means the EM field satisfies the Bloch periodic boundary condition. Even though the results of FDTD much like that of analytical method, the small difference between analytical calculation and FDTD is explained by the multiple order terms ($\mathrm{abs}(n) > 0$) in (5). In Fig. 1(a), we disregard the high-order terms ($\mathrm{abs}(n) > 0$) in (6) and (7), thus pulling up the dispersion curve.

III. DISPERSION DIAGRAM OF SSPP ALONG THE SANDWICHED METAMATERIAL

In the previous section, it has been shown that the SSPP bound modes in a corrugated perfect conductor can be controlled by changing the refractive index of the grooves. We now focus on a realistic THz micrometer-scale switch device. The inset of Fig. 2(a) shows a schematic picture of an active THz plasmon switch consisting of a dielectric plasmon gap between two corrugated perfect metamaterials with geometrical parameters $a/d = 0.1$, $h/d = 0.5$, and $t/d = 1/3$, thus confining the localized THz pulse and demonstrating the highly miniaturized active THz switch. For a complex geometry, the SSPP dispersion curves and mode profiles of the sandwiched structure can be obtained by FDTD. In contrast to 1-D corrugated structure, the sandwiched structure exhibits interesting features [17]. To be specific, the reflection symmetry through the plane $z = 0$ generates multiple SSPP modes along the signal line, as shown in Fig. 2(a). The dispersion of first-band mode closely matches with that of 1-D array grooves calculated from (7). In addition, the periodic x-directional transition symmetry creates the SSPP band-gap similar to photonic crystals. Furthermore, the second mode with a flatband is located at the region between the SSPP band-gap. Thus, this mode becomes a slow light in which the velocity of SSPP modes physically can be lowered. Furthermore, slow light enabled by resonant mode operation is promising method for shrinking the size of THz devices and controlling THz signal in the time domain [20]. In contrast to periodic dielectric ($n > 0$) waveguide, the resonant frequency exists in the region of second-band mode. As shown in Fig. 2(b), the existence of structural resonant modes can be understood intuitively by considering the unit periodic cell act like a THz cavity with small quality factor Q and periodic unit cells are connected to each other with coupling coefficient. Physically, the periodic dielectric corrugated gap structure with refractive index ($n > 0$) cannot support the localized field because of the boundary condition. However, the
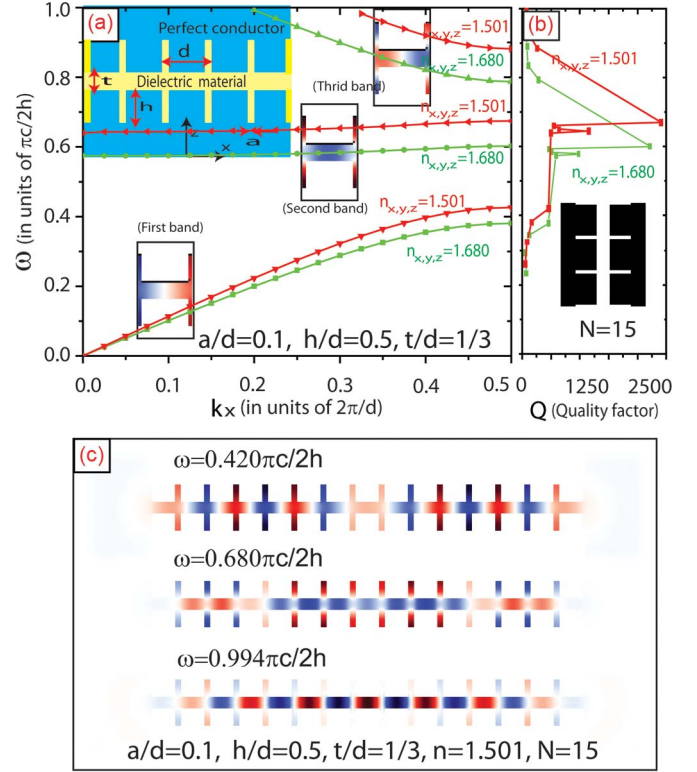

Fig. 2. (a) Dispersion diagram of SSPP bound modes supported by the sandwiched conductor metamaterials with geometrical parameters $a/d = 0.1$, $h/d = 0.5$, and $t/d = 1/3$. (b) Quality factor Q for SSPP switch with the grooves ($N = 15$) is obtained by FDTD. (c) Mode profiles for SSPP switch with the grooves ($N = 15$) at three different operating frequencies: first-band mode ($\omega = 0.420\,\pi c/2h$), second-band mode ($\omega = 0.680\,\pi c/2h$), and third-band mode ($\omega = 0.994\,\pi c/2h$).

metallic structure provides the structural resonant frequency, thus supporting confined SSPP modes, as shown in Fig. 2(a).

To obtain an efficient THz switch, we focus on the resonant SSPP modes for two fundamental reasons: small damping mechanism and strong SSPP confinement. First, to verify the small damping system at resonant frequency, we conduct the computation of the quality factor $Q \approx \omega_0/\gamma$ where γ is the loss rate. The quality factor Q is useful in determining the system behavior in the resonant system. In our system, the net dimensionless decay rate can be rewritten as sum of two dominant decay rates: $1/Q = 1/Q_r + 1/Q_w$, where $1/Q_r$ and $1/Q_w$ denotes the radiative and waveguide decay rates, respectively. To eliminate the radiative loss and estimate the waveguide decay, we excite the Gaussian point source at the center of sandwiched structure with groove numbers ($N = 15$) and analyze the response with the help of filter diagonalization method [21]. In this case, Q has a sharp peak at the specific frequency, thus verifying resonant modes and narrow bandpass filter. Similar to the extraordinary transmission of subwavelength metallic holes [22], [23], the enhanced transmission through a corrugated sandwiched structure can be achieved by operating the resonant mode. Second, to demonstrate the subwavelength SSPP confinement at the resonant modes, the field profiles at three different frequencies are shown in Fig. 2(c). These figures show the magnetic-field (H_z) patterns of states localized about a corrugated metallic gap. By examining the field profiles, the first-band mode ($\omega = 0.420\ \pi c/2h$) shows the equally field

distribution in the y–z plane. However, the third-band mode ($\omega = 0.994\ \pi c/2h$) exhibits the alternating two different field concentrations in the y–z domain. In particular, at the second-band mode (resonant mode: $\omega = 0.680\ \pi c/2h$), the EM fields are mainly concentrated on the grooves, thus demonstrating strong SSPP subwavelength localization. Therefore, these features increase the high EM field intensity and sensitivity in a small volume, thus enhancing nonlinear optical effects for THz active devices such as switch and multiplexer.

In addition, for a more practical THz design, we need to optimize guiding parameters that SSPP resonant modes are located in the THz domain. The key design rule is that SSPP resonant frequency is inversely proportional to the refractive index (n) and height (h) as similar to cutoff frequency $\omega_c = \pi c/2n_x h$ in the 1-D SSPP structure. Fig. 3(a) shows the TM dispersion relations of sandwiched conductor metamaterial supported by geometrical conditions: $a = 6\ \mu$m, $d = 60\ \mu$m, $h = 30\ \mu$m, and $t = 20\ \mu$m. In detail, at $n = 1.501$ and $n = 1.680$, the resonant frequencies are about $\omega = 1.60$ THz and $\omega = 1.45$ THz, respectively. This resonant frequency modulation in our THz architecture enables us to control or steer the THz signal by manipulating the refractive indices of periodic grooves.

IV. ACTIVE SPOOF THz SWITCH BASED ON METAMATERIAL

In this section, we apply the theoretical approach to practical implementation. To turn signal lines ON and OFF based on a shift of resonance frequency, a large birefringence is warranted at a low control signal, thus offering significant flexibility into existing optoelectronic devices. For example, the refractive index change can be achieved by several methods such as conventional electrooptic and nonlinear optical bistable material. In this paper, we introduce the N-LC with the dielectric anisotropy defining as $\Delta n = n_e - n_o$, where n_e and n_o are refractive indexes parallel and perpendicular to the molecular axis [24], [25]. Furthermore, the LC birefringence can be easily controlled by changing alignment of LC based on a low voltage. In this way, the orientations of LC induced by electric field or optical excitation determine the three fundamental refractive indices of x-, y-, and z-axis, thus modifying the artificially engineered SSPP modes in the active THz switch.

To confirm the active switching operating at THz frequency based on the LC orientations, we conducted HFSS simulation based on the finite-element method (FEM). In the FDTD simulation, we investigated the basic principles of SSPP guiding 2-D structure based on the isotropic medium. However, in the FEM simulation, for a more realistic physical model, we designed a 3-D THz switch. The spatial snapshots of magnitude E field in the x–z plane along the active 3-D finite THz switch, as shown in Fig. 3(b)–(d). Basically, the 2-D structure has one mirror symmetry plane $z = 0$, thus classifying the TM modes and TE modes. However, the 3-D structure has two mirror symmetry plane $z = 0$ and $y = 0$, thus all modes have symmetric (even) and antisymmetric (odd) with respect to two planes. Therefore, the guiding width w is important factor to determine the dispersion curve and resonant frequency. For example, for the case of thin structure with small width w,
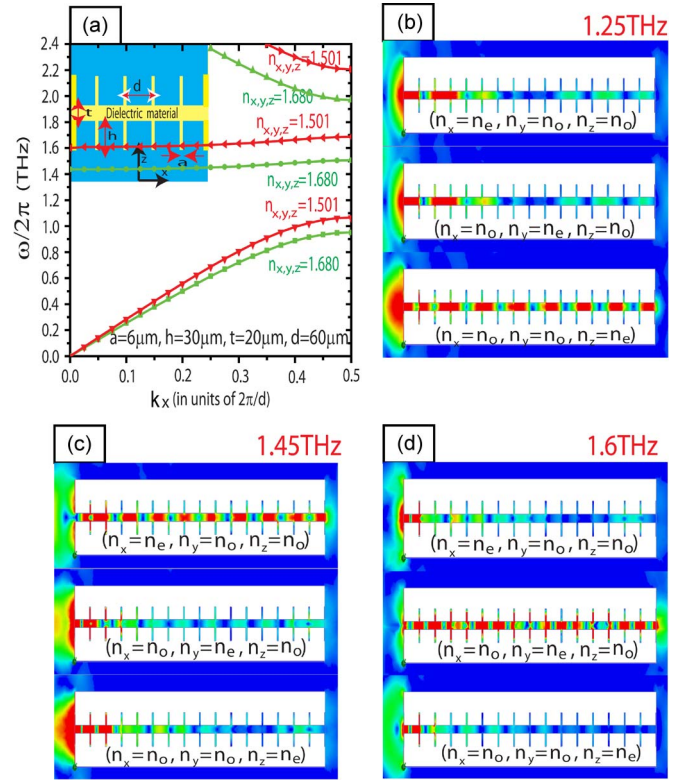

Fig. 3. (a) Dispersion graphs of the spoof surface plasmon supported by the sandwiched conductor metamaterial with geometrical parameters for $a = 6\ \mu$m, $d = 60\ \mu$m, $h = 30\ \mu$m, and $t = 20\ \mu$m. (b)–(d) Spatial distributions of the E-field along the active THz switch devices for three different fundamental LC orientations at 1.25, 1.45, and 1.6 THz, respectively. The geometrical configurations for $a = 6\ \mu$m, $d = 60\ \mu$m, $h = 30\ \mu$m, $t = 20\ \mu$m, $n_o = 1.501$, and $n_e = 1.680$.

the EM field modes are imposed by the two mirror symmetric conditions ($z = 0$ and $y = 0$). However, for the case of thick structure with large width w, the EM field modes almost constrained by the one mirror symmetric condition ($z = 0$). To verify the previous analytical method based on 2-D analysis, we use large width $w = 160\ \mu$m (y-direction) and the structure has the same geometrical parameters of 2-D guiding structure containing 16 grooves. Furthermore, contrast to FDTD simulation, we use biaxial medium from N-LC with $n_o = 1.501$ and $n_e = 1.680$ [26]. Therefore, we consider three fundamental LC orientations: ($n_x = n_e, n_y = n_o, n_z = n_o$), ($n_x = n_o, n_y = n_e, n_z = n_o$), and ($n_x = n_o, n_y = n_o, n_z = n_e$). As expected from the TM dispersion analysis, the THz guided wave along the guiding gap is engineered by different LC orientations. In particular, at 1.6 THz, the y alignment ($n_y = n_e$) of LC generates strongly coupled SSPP resonant modes, thus meaning ON-state. This field pattern is very similar to the resonant mode of FDTD simulation, as shown in Fig. 2(c). This extraordinary transmission can be explained by TM dispersion analysis, as shown in Fig. 3(a), because the SSPP modes based on the anisotropic medium are constrained by n_x and n_z as illustrated in (7). Therefore, the THz guided wave can be characterized by the isotropic medium ($n = 1.501$), thus the resonant modes are located at 1.6 THz. On the other hand, x or z alignment of LC prohibits THz pulse signal about the metamaterials, thus denoting OFF-state.
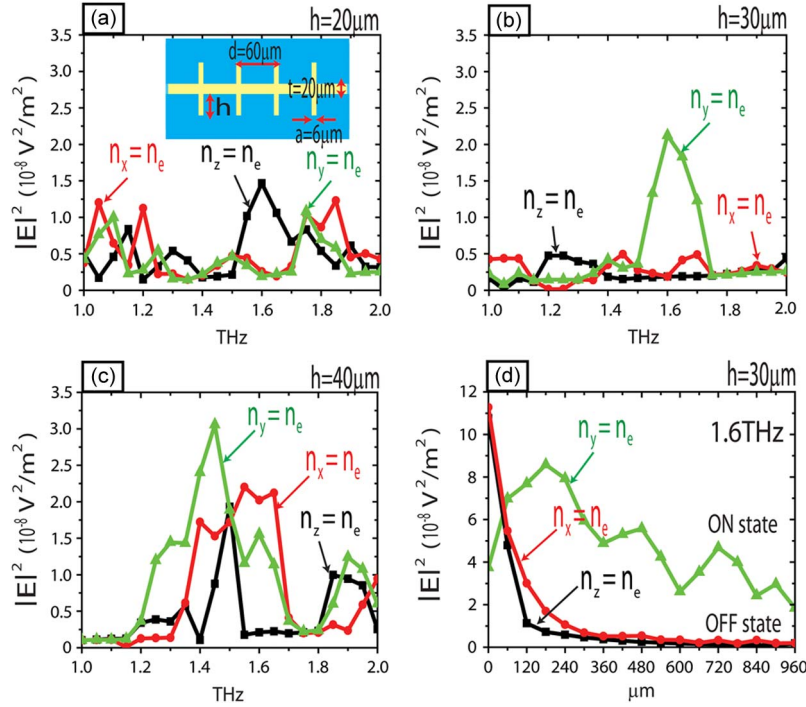
Fig. 4. (a)–(c) E field amplitude versus frequency calculated at the output of THz switch in which the periodic lattice ($d = 60\ \mu$m) and groove width ($a = 6\ \mu$m) are fixed, and at the heights of 20, 30, and 40 μm, respectively. (d) Magnitude of E field, evaluated at $f = 1.6$ THz, along the x-direction at different locations of the metamaterials corresponding to three different fundamental LC orientations.

In order to obtain the optimal THz switching, Fig. 4(a)–(c) shows the E field amplitude calculated at the output of THz switch in which the periodic lattice ($d = 60\ \mu$m), groove width ($a = 6\ \mu$m), and thickness ($t = 20\ \mu$m) are fixed, and at the heights (h) of 20, 30, and 40 μm, respectively. As shown, the transmittance of the SSPP bound modes along the plasmonic gap can be controlled by the guiding geometry, operation frequency f, and refractive index n [18]. Additionally, a dramatic dependence of the height of the corrugated structure is clearly visible. The increase in E magnitude with increasing height between 1 and 2 THz is due to the large depth of indentation leading to strong EM field penetration into the metallic side. Furthermore, the optimal guiding switching can be obtained at 1.6 THz with $h = 30\ \mu$m, thus obtaining approximately maximum 10.51-dB extinction ratio defined as $r_e = 10\log(P_{\mathrm{ON}}/P_{\mathrm{OFF}})$ with ON-state (Y alignment) and OFF-state (X or Z alignment), as shown in Fig. 4(b). In addition, Fig. 4(d) shows the signal attenuation at different locations of metamaterials with a height of 30 μm at 1.6 THz corresponding to three different LC orientations. As apparent from the figure, the extraordinary SSPP resonance between grooves, in the ON (Y alignment)-state, leads to small signal attenuation, thus having 3.21 dB/cm. However, in the OFF-state (X or Z alignment), the signal loss is almost equal to 18.51 dB/cm.

More importantly, this simple linear structure designed for the optimal switching condition can be easily extended to more complex logic elements. Fig. 5(a) shows the equivalent circuit model of a Y-junction THz switch containing four grooves in each section and independent control signal line. As shown in Fig. 5(b), this THz circuit model can be easily realized by manipulating the combination sets of LC orientation. In the case
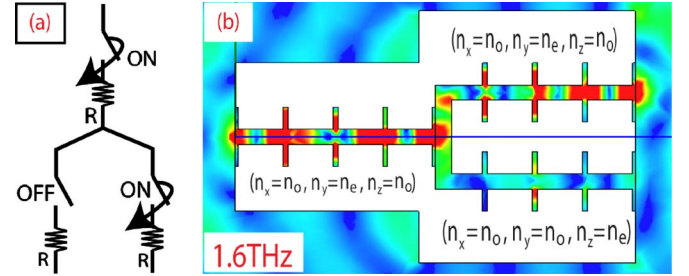

Fig. 5. (a) Equivalent circuit of the THz Y-junction switch with three control signals. (b) Spatial distributions of the E-field along the active Y-junction THz switch with geometrical configurations for $a = 6\ \mu$m, $d = 60\ \mu$m, $h = 30\ \mu$m, and $t = 20\ \mu$m at 1.6 THz.

of Y-junction switching, we can obtain intuitively understanding of signal transmission by applying coupled mode theory. Since each junction can be considered as a weak resonant cavity which is adjacent to THz waveguides, the transmission in ON-state or OFF-state depends on the specific junction geometry. In practical realizations, we need to consider the impedance matching issues between each junctions and THz corrugated waveguides. Additionally, the signal lines consisting of small grooves can solve the possible issues such as uniform LC alignment under an electric field or inherent LC damping. Furthermore, the geometry is simple to fabricate and can be easily implemented to execute THz Boolean logic algorithm.

V. CHALLENGES AND SUMMARY

In this paper, we have demonstrated that active control of SSPP signal at THz frequencies can be accomplished by modulating the refractive index of N-LC material. However, further
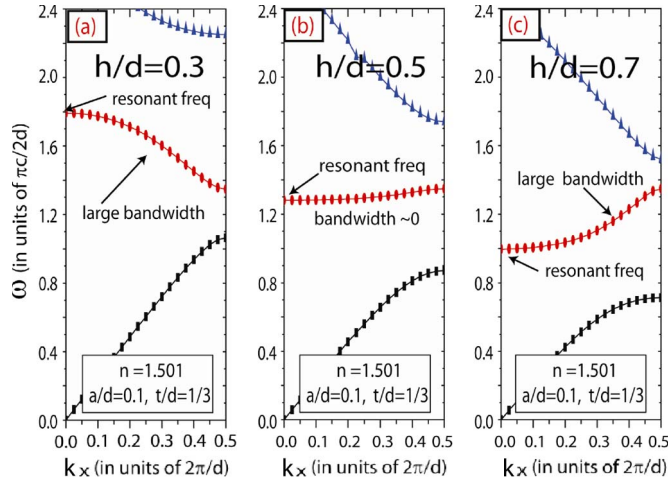
Fig. 6. Dispersion diagram of SSPP bound modes supported by the sandwiched conductor metamaterials with geometrical parameters $a/d = 0.1$, $t/d = 1/3$, and $n = 1.501$ for three different choices of h/d. (a) At $h/d = 0.3$, the bandwidth of second band is large. (b) At $h/d = 0.5$, the bandwidth goes to zero. (c) At $h/d = 0.7$, the bandwidth of second band is large.

Fig. 7. Schematic of the THz Y-junction switching: electric contacts placed directly onto the electrically disconnected metallic lines.

consideration must be given for practical implementation of the core idea proposed in this paper.

1) First, the main physical issue stems from limited bandwidth [27]. In principle, dramatic signal slow down and efficient energy transfer can be achieved by using resonant modes. However, the operation of resonance modes imposes significant bandwidth constraints, thereby limiting the range of available operational frequencies. For example, as shown in Fig. 2(a), the bandwidth of second-band mode is almost zero. To increase the bandwidth of second-band mode, we can design the bandwidth by choosing appropriate waveguide structures. For example, we can change geometrical parameter h/d based on the guiding parameters $a/d = 0.1$, $t/d = 1/3$, and $n = 1.501$, as shown in Fig. 6. More specifically, for small height $h/d = 0.3$ and large height $h/d = 0.7$, the bandwidth of second mode is large. However, for medium height $h/d = 0.5$, the bandwidth of second mode goes to zero, thus compressing the bandwidth of THz pulse, as shown in Fig. 6(b). Even though bandwidth compression enables designers to spatially compress the pulsewidth and increase the internal fields, the small bandwidth is not desirable in THz applications. Therefore, it is essential to consider the delay-bandwidth product for an efficient THz switching device [28].

2) Second, the switching speed of LC is significantly lower than conventional EO materials such as KH_2PO_4 or $LiNbO_3$. This difficulty can be addressed by using other methods such as nonlinear EO, optically controlled, or loss-induced material [29]. Recently, SPP signals in metallic on dielectric waveguides can be controlled by using the phase transition of crystalline gallium [18]. As an alternative for SSPP routing, this phase transition owing to the temperature change or external optical excitation provides strong modulation strength ($\delta n/n$) and relatively fast switching speed.

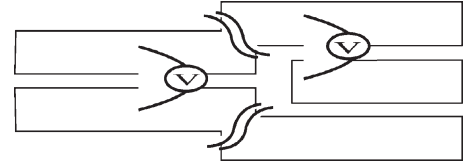3) Third, the inherent attenuation of LC in the THz domain may have an influence on SSPP dispersion, thereby

changing resonant modes, bandwidth and quality factor (Q). In general, the SSPP dispersion mode strongly depends on the dispersive modulation (δn) and absorptive modulation ($\delta \alpha$). Since absorption is strongly related to signal attenuation, absorption modulation is not broadly considered as a switching mechanism. However, absorption modulation ($\delta \alpha$) may extend the degree of freedom for signal routing similar to absorptive optical bistability method.

4) Fourth, the device performance depends on the polarization of the incident THz field. Therefore, the THz circuit system requires the TM polarizer at the input port.

5) Fifth, the insertion loss at the input port has a large value because the input port and subwavelength gap structure have a significant impedance mismatch. To decrease the momentum mismatch, we can design the THz waveguide or switching system with a periodic arrangement of cut-through corrugated slits [30]. This arrangement may lead to solve the momentum mismatch between the gap structure and input port.

6) Finally, the device implementation such as electrical contacts cannot be easily made. For example, in the case of Y-junction switch, if we assume that the electric contacts placed directly onto corrugated metallic structures, the metallic structure has physically the same voltage value. To obtain the different voltage configurations between signal lines, the device designers need to obtain electrically disconnected metallic lines, as shown in Fig. 7. In addition, electric contacts in the immediately vicinity of confined SSPP modes may result in additional signal loss. Therefore, it is essential to find a way to minimize the signal loss.

However, even though there remain many unresolved challenges to design experimental plasmon logic gates, the basic method presented here provides promising possibilities for the active THz device occupying an area of several micrometer-meters square. In particular, the proposed linear Y-junction switching devices operate as a 2 : 1 multiplexer, a fundamental building block in the digital systems. This paper concludes that the unique properties of SSPP modes having strong subwavelength EM confinement, low signal attenuation, and high extinction ratio will open a new vista for the next generation subwavelength active THz devices.

APPENDIX
NORMAL SURFACE OF ANISOTROPIC MEDIA

We assume a monochromatic plane wave of angular frequency ω propagating in anisotropic medium with an electric

field and a magnetic field

$$E \exp\left[i(\omega t - k \cdot r)\right]$$

$$H \exp\left[i(\omega t - k \cdot r)\right].$$

From the Maxwell equation, we obtain

$$k \times (k \times E) + \omega^2 \mu \varepsilon E = 0.$$

The fundamental dielectric tensor ε is given by $\epsilon = (\epsilon_x, \epsilon_y, \epsilon_z)$. This leads to a constitutive relation between ω and k

$$\det \begin{vmatrix} \omega^2 \mu \varepsilon_x - k_y^2 - k_z^2 & k_x k_y & k_x k_z \\ k_y k_x & \omega^2 \mu \varepsilon_y - k_y^2 - k_z^2 & k_y k_z \\ k_z k_x & k_z k_y & \omega^2 \mu \varepsilon_z - k_y^2 - k_z^2 \end{vmatrix} = 0.$$

In the case of $k_y = 0$, we obtain two normal surfaces

$$\left(k_{x,I}^{(n)2} + k_{z,I}^{(n)2}\right) / n_y^2 = (\omega/c)^2 : \text{TE polarization}$$

$$\left(k_{x,I}^{(n)}/n_z\right)^2 + \left(k_{z,I}^{(n)}/n_x\right)^2 = (\omega/c)^2 : \text{TM polarization}.$$

ACKNOWLEDGMENT

REFERENCES

[1] P. H. Siegel, "Terahertz technology," *IEEE Trans. Microw. Theory Tech.*, vol. 50, no. 3, pp. 910–928, Mar. 2002.

[2] R. Kohler, A. Tredicucci, F. Beltram, H. E. Beere, E. H. Linfield, A. G. Davies, D. A. Ritchie, R. C. Iotti, and F. Rossi, "Terahertz semiconductor-heterostructure laser," *Nature*, vol. 417, no. 6885, pp. 156–159, May 2002.

[3] D. M. Mittleman, R. H. Jacobsen, and M. C. Nuss, "T-ray imaging," *IEEE J. Sel. Topics Quantum Electron.*, vol. 2, no. 3, pp. 679–692, Sep. 1996.

[4] Q. Cao and J. Jahns, "Azimuthally polarized surface plasmons as effective terahertz waveguides," *Opt. Express*, vol. 13, no. 2, pp. 511–518, Jan. 2005.

[5] K. L. Wang and D. M. Mittleman, "Metal wires for terahertz wave guiding," *Nature*, vol. 432, no. 7015, pp. 376–379, Nov. 2004.

[6] J. B. Pendry, L. Martin-Moreno, and F. J. Garcia-Vidal, "Mimicking surface plasmons with structured surfaces," *Science*, vol. 305, no. 5685, pp. 847–848, Aug. 2004.

[7] A. P. Hibbins, B. R. Evans, and J. R. Sambles, "Experimental verification of designer surface plasmons," *Science*, vol. 308, no. 5722, pp. 670–672, Apr. 2005.

[8] G. Goubau, "Surface waves and their application to transmission lines," *J. Appl. Phys.*, vol. 21, no. 11, pp. 1119–1128, Nov. 1950.

[9] R. Elliott, "On the theory of corrugated plane surfaces," *Trans. IRE Prof. Group Antennas Propag.*, vol. 2, no. 2, pp. 71–81, Apr. 1954.

[10] W. Rotman, "A study of single-surface corrugated guides," *Proc. IRE*, vol. 39, no. 8, pp. 952–959, Aug. 1951.

[11] S. A. Maier and S. R. Andrews, "Terahertz pulse propagation using plasmon-polariton-like surface modes on structured conductive surfaces," *Appl. Phys. Lett.*, vol. 88, no. 25, p. 251 120, Jun. 2006.

[12] S. A. Maier, S. R. Andrews, L. Martin-Moreno, and F. J. Garcia-Vidal, "Terahertz surface plasmon-polariton propagation and focusing on periodically corrugated metal wires," *Phys. Rev. Lett.*, vol. 97, no. 17, p. 176 805, Oct. 2006.

[13] T. W. Ebbesen, C. Genet, and S. I. Bozhevolnyi, "Surface-plasmon circuitry," *Phys. Today*, vol. 61, no. 5, pp. 44–50, May 2008.

[14] A. V. Krasavin and N. I. Zheludev, "Active plasmonics: Controlling signals in Au/Ga waveguide using nanoscale structural transformations," *Appl. Phys. Lett.*, vol. 84, no. 8, pp. 1416–1418, Feb. 2004.

[15] D. E. Chang, A. S. Sorensen, E. A. Demler, and M. D. Lukin, "A single-photon transistor using nanoscale surface plasmons," *Nat. Phys.*, vol. 3, no. 11, pp. 807–812, 2007.

[16] J. G. Rivas, J. A. Sanchez-Gil, M. Kuttge, P. H. Bolivar, and H. Kurz, "Optically switchable mirrors for surface plasmon polaritons propagating on semiconductor surfaces," *Phys. Rev. B, Condens. Matter Mater. Phys.*, vol. 74, no. 24, p. 245 324-6, Dec. 2006.

[17] B. W. Wang, Y. Jin, and S. L. He, "Design of subwavelength corrugated metal waveguides for slow waves at terahertz frequencies," *Appl. Opt.*, vol. 47, no. 21, pp. 3694–3700, Jul. 2008.

[18] A. P. Hibbins, M. J. Lockyear, and J. R. Sambles, "The resonant electromagnetic fields of an array of metallic slits acting as Fabry–Pérot cavities," *J. Appl. Phys.*, vol. 99, no. 12, p. 124 903, Jun. 2006.

[19] F. J. Garcia-Vidal, L. Martin-Moreno, and J. B. Pendry, "Surfaces with holes in them: New plasmonic metamaterials," *J. Opt. A, Pure Appl. Opt.*, vol. 7, no. 2, pp. S97–S101, Feb. 2005.

[20] Y. A. Vlasov, M. O'Boyle, H. F. Hamann, and S. J. McNab, "Active control of slow light on a chip with photonic crystal waveguides," *Nature*, vol. 438, no. 7064, pp. 65–69, Nov. 2005.

[21] A. Farjadpour, D. Roundy, A. Rodriguez, M. Ibanescu, P. Bermel, J. D. Joannopoulos, S. G. Johnson, and G. W. Burr, "Improving accuracy by subpixel smoothing in the finite-difference time domain," *Opt. Lett.*, vol. 31, no. 20, pp. 2972–2974, Oct. 2006.

[22] T. W. Ebbesen, H. J. Lezec, H. F. Ghaemi, T. Thio, and P. A. Wolff, "Extraordinary optical transmission through sub-wavelength hole arrays," *Nature*, vol. 391, no. 6668, pp. 667–669, Feb. 1998.

[23] Z. Ruan and M. Qiu, "Enhanced transmission through periodic arrays of subwavelength holes: The role of localized waveguide resonances," *Phys. Rev. Lett.*, vol. 96, no. 23, p. 233 901-4, Jun. 2006.

[24] A. L. Zhang, K. T. Chan, M. S. Demokan, V. W. C. Chan, P. C. H. Chan, H. S. Kwok, and A. H. P. Chan, "Integrated liquid crystal optical switch based on total internal reflection," *Appl. Phys. Lett.*, vol. 86, no. 21, p. 211 108, May 2005.

[25] M. Kobayashi, H. Terui, M. Kawachi, and J. Noda, "2 × 2 optical-waveguide matrix switch using nematic liquid-crystal," *IEEE J. Quantum Electron.*, vol. QE-18, no. 10, pp. 1603–1610, Oct. 1982.

[26] F. Zhang, Q. Zhao, L. Kang, D. P. Gaillot, X. Zhao, J. Zhou, and D. Lippens, "Magnetic control of negative permeability metamaterials based on liquid crystals," *Appl. Phys. Lett.*, vol. 92, no. 19, p. 193 104-3, May 2008.

[27] T. Baba, "Slow light in photonic crystals," *Nat. Photon.*, vol. 2, no. 8, pp. 465–473, Aug. 2008.

[28] M. F. Yanik, W. Suh, Z. Wang, and S. Fan, "Stopping light in a waveguide with an all-optical analog of electromagnetically induced transparency," *Phys. Rev. Lett.*, vol. 93, no. 23, p. 233 903, Dec. 2004.

[29] M. Soljačić, M. Ibanescu, S. G. Johnson, Y. Fink, and J. D. Joannopoulos, "Optimal bistable switching in nonlinear photonic crystals," *Phys. Rev. E, Stat. Phys. Plasmas Fluids Relat. Interdiscip. Top.*, vol. 66, no. 5, p. 055 601, Nov. 2002.

[30] J. T. Shen, P. B. Catrysse, and S. Fan, "Mechanism for designing metallic metamaterials with a high index of refraction," *Phys. Rev. Lett.*, vol. 94, no. 19, p. 197 401, May 2005.
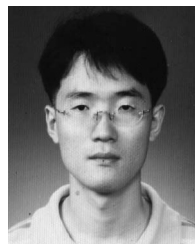
Kyungjun Song received the B.S. degree in mechanical engineering from Seoul National University, Seoul, Korea, in 2002 and the M.S. degree in mechanical engineering from the University of Michigan, Ann Arbor, in 2004, where he is currently working toward the Ph.D. degree.

He is a Graduate Student Research Assistant with the Electrical Engineering and Computer Science Department, University of Michigan. His current research interests include the modeling, simulation, and design of plasmonic nanoarchitecture.

Pinaki Mazumder (F'99) received the Ph.D. degree from the University of Illinois at Urbana–Champaign, Urbana, in 1988.

He is currently a Professor with the Department of Electrical Engineering and Computer Science, University of Michigan (UM), Ann Arbor. He is on leave for one year from the UM to serve as the lead Program Director of the Emerging Models and Technologies Program with the U.S. National Science Foundation, Arlington, VA. He was for six years with industrial R&D centers that included AT&T Bell Laboratories, where in 1985, he started the CONES Project-the first C modeling-based very large scale integration (VLSI) synthesis tool at India's premier electronics company, Bharat Electronics, Ltd., where he had developed several high-speed and high-voltage analog integrated circuits intended for consumer electronics products. He is the author or coauthor of more than 200 technical papers and four books on various aspects of VLSI research works. His current research interests include current problems in nanoscale CMOS VLSI design, computer-aided design tools, and circuit designs for emerging technologies including quantum MOS and resonant tunneling devices, semiconductor memory systems, and physical synthesis of VLSI chips.

Dr. Mazumder is an American Association for the Advancement of Science Fellow (2008). He was a recipient of the Digital's Incentives for Excellence Award, BF Goodrich National Collegiate Invention Award, and Defense Advanced Research Projects Agency Research Excellence Award.